MODELLING LOW-VELOCITY IMPACT DAMAGE BEHAVIOR OF FIBER-REINFORCED COMPOSITES USING COMBINED CONTINUUM AND DISCRETE DAMAGE MODELING TECHNIQUES

Shabani, P.[1], Qi, G.[2], Li, L.[2]*, Laliberté, J.[1]**
[1] Department of Mechanical and Aerospace Engineering, Carleton University, 1125 Colonel By Drive, Ottawa, ON K1S 5B6, Canada
[2] Aerospace Research Centre, National Research Council Canada, 1200 Montreal Road, Ottawa, ON K1A 0R6, Canada
* Corresponding author (Lucy.Li@nrc-cnrc.gc.ca)
** Corresponding author (Jeremy.Laliberte@carleton.ca)

Keywords*: Composites; Low-velocity impact; damage modeling.*

ABSTRACT

Low-velocity impact (LVI) damage may occur during fabrication process and throughout the service life of composite structures. It is important to have a reliable computational model to predict the damage evolution to guide the design of a composite structure that is prone to impact damage. The objective of the current research was to develop an effective modeling methodology to predict the response of composite laminates subjected to LVI and monitor the damage evolution inside the laminates. To this end, a finite element (FE) model was developed with Abaqus using combined discrete and continuum damage modeling techniques. The cohesive zone modeling technique was employed to capture both interlaminar delamination and intralaminar matrix cracking. A VUMAT user subroutine based on the 3-D Hashin's failure criteria was written and integrated into the FE model to predict the fiber breakage and transverse matrix cracking. The developed modeling methodology was applied to a 254 mm × 305 mm (10 in × 12 in) carbon fiber-reinforced epoxy (IM7/977-3) laminate with a stacking sequence of $[0/45/90/-45]_{4s}$ subjected to 30 J impact with a 15.87 mm diameter hemispherical impactor. The computational results were validated by the experiments with good agreement. In the design of a composite structure, it is helpful to know when and where the damage would initiate in order to strengthen the weak areas. For this purpose, the histories of dissipated energies due to different types of damage were recorded at each ply and inter-ply (cohesive layer). With these data, the evolution of the damage can be precisely traced inside the laminate, and the stiffness degradation in each ply can be correlated with the corresponding damage formation event.

1 INTRODUCTION

Low-velocity impact (LVI) at a low energy level can cause small or even barely visible impact damage in a composite laminate. Although the damage might be barely visible to visual inspection, it can result in a significant reduction in the mechanical properties of the impacted structure. To predict the damage evolution in a composite laminate during a low-velocity impact event, many numerical models have been proposed [1-6]. Some models employed the continuum damage mechanics (CDM) approach to model damage initiation and propagation [7-9], while others considered a discrete representation [1-2, 6, 10-13]. In the CDM models, a lower number of elements is adequate. Hence, they take less computational time to simulate the response of the laminate under LVI compared with discrete models. In the discrete models, cohesive elements are embedded between every two composite plies to predict

delamination [2, 3, 5, 14], and cohesive elements may also be deployed inside each of the composite plies to model intralaminar matrix cracking [1, 10, 13, 15-16]. Discrete models are more complex with high computational costs. However, they usually provide a more accurate prediction for damage evolution. In the current research, a modeling methodology with the combination of continuum and discrete representation of composite damage was developed. The finite element model was validated by LVI experiments on composite laminates with a stacking sequence of $[0/45/90/-45]_{4s}$ subjected to 30 J impact energy.

2 DAMAGE MODELING STRATEGY

2.1 Damage Modeling Using Cohesive Zone Method (CZM)

A three-dimensional finite element (FE) modeling was carried out using Abaqus/CAE and solved by its explicit solver to predict the low-velocity impact response of a composite laminate. A 254 mm × 304.8 mm (10 in × 12 in) laminate with a stacking sequence of $[0/45/90/-45]_{4s}$ was impacted by a spherical impactor with a diameter of 15.87 mm (0.625 in), as shown in Figure 1(a). The FE model aimed to predict the damage evolution in each ply during the impact and to predict the force-time and displacement-time histories of the laminate. Each of the composite layers had a thickness of 0.131 mm and was modeled using 3D solid elements (C3D8R). To capture delamination between each of the composite layers, a cohesive element layer with a thickness of 0.005 mm was added between composite plies as illustrated in Figure 1(c). In addition, inside each of the composite layers, 6 rows of cohesive elements were embedded to capture intralaminar matrix cracking and they were placed surrounding the impact region, which was more prone to damage. The thickness of these cohesive rows was 0.02 mm and they were placed at a distance of 7.62 mm from each other. These rows of elements are illustrated in Figure 1 (b) and (d). The mesh distributions in the cohesive layers and the composite layers with different fiber orientations are shown in Figure 1(e). To ensure computational convergence and sufficient solution accuracy in the region near the impactor tip, finer meshes were developed in that region.

The mechanical properties of the carbon fiber-reinforced epoxy (IM7/977-3) composite laminate, cohesive layer, and the clamping rubber are summarized in Table 1. Among the cohesive properties, α represents the power of the power-law that describes the mixed-mode fracture behavior, as shown in Eq. (1).

$$\left(\frac{G_I}{G_{IC}}\right)^{\alpha} + \left(\frac{G_{II}}{G_{IIC}}\right)^{\alpha} + \left(\frac{G_{III}}{G_{IIIC}}\right)^{\alpha} = 1 \tag{1}$$

Proper boundary condition setup is the key to achieving a convergent solution for this complex problem. To prevent rigid body motions of the laminate in the in-plane (X and Y) directions, contact interactions were defined between the edges of the laminate and the positioning pins on the support plate. Contact was also defined between the support plate and the bottom surface of the laminate, while the supporting plate and the impactor were considered as rigid bodies. In addition, four rubber clamps were utilized (green cylinders in Figure 1(a)) to damp the vibration of the laminate after the impact event, and thus contact interactions were created between the bottom surfaces of the rubber clamps and the top surface of the laminate. The top surfaces of the four rubber clamps were assigned "fixed" boundary conditions to stabilize the entire structure. To build interactions among the composite layers due to their nonconforming mesh patterns, "tie constraints" were established between each cohesive element layer and its neighboring composite layers. Since the "element deletion" was activated for the cohesive elements, additional contacts were defined among all the composite layers to avoid their penetration after the failure of the embedded cohesive layers.

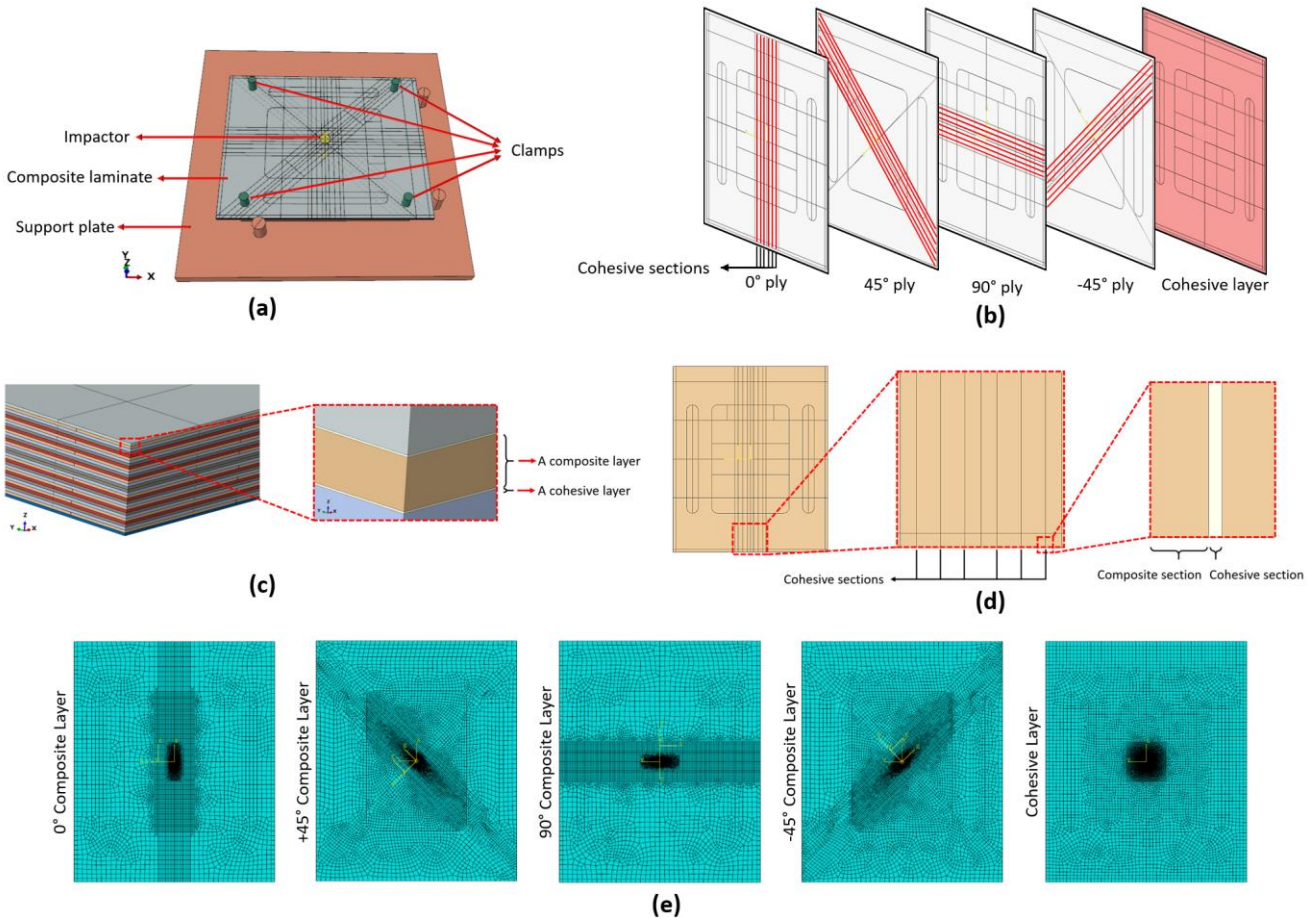

Figure 1. (a) Assembled FE model for low-velocity impact test; (b) Embedded cohesive elements in the FE model; (c) Modeled composite laminate with cohesive layers; (d) Cohesive sections embedded in a 0° composite layer; (e) Mesh distributions in different layers of the model.

2.2 Damage Modeling Using Continuum Damage Mechanics (CDM)

Using cohesive elements, the proposed FE model can catch delamination and intralaminar matrix cracking at predefined locations. However, it cannot capture other damage modes, such as fiber breakage. Also, since the locations of the intralaminar matrix cracks are predefined, it cannot predict the occurrence of matrix cracking at other regions. To be able to capture fiber breakage and matrix cracking in all potential regions of the composite laminate, a VUMAT user subroutine was developed based on the 3-D Hashin's failure criteria [17] and was implemented during the Abaqus solution process. To test the validity of the VUMAT, a simplified impact model without cohesive zones was created, as shown in Figure 2(a). The results of this model had overall good agreement with the experiment (Figure 2(b)-(d)), demonstrating the effectiveness of the VUMAT. Meanwhile, the discrepancies shown in the figure were also expected due to the limitations of the simplified model.

Table 1. Mechanical properties of the different parts used in the model.

Carbon/Epoxy (IM7/977-3)									
ρ (Kg/m^3)	E_{11} (GPa)	E_{22} (GPa)	E_{33} (GPa)	G_{12} (GPa)	G_{13} (GPa)	G_{23} (GPa)	ν_{12}	ν_{13}	ν_{23}
1596	157.50	8.97	8.88	5.67	5.21	3.14	0.320	0.329	0.461
X_T (MPa)	X_C (MPa)	Y_T (MPa)	Y_C (MPa)	S_L (MPa)	S_T (MPa)				
2703.9	1764.2	95.6	236.5	117.9	104.7				
Rubber									
ρ (Kg/m^3)	E (GPa)	ν							
1520	863	0.4							
Cohesive Properties									
ρ (Kg/m^3)	E (N/mm^3)	T_n (MPa)	T_s (MPa)	T_t (MPa)	G_{IC} (N/mm)	G_{IIC} (N/mm)	G_{IIIC} (N/mm)	α	
1320	5000	77.23	60.00	60.00	0.216	0.607	1.272	2.284	

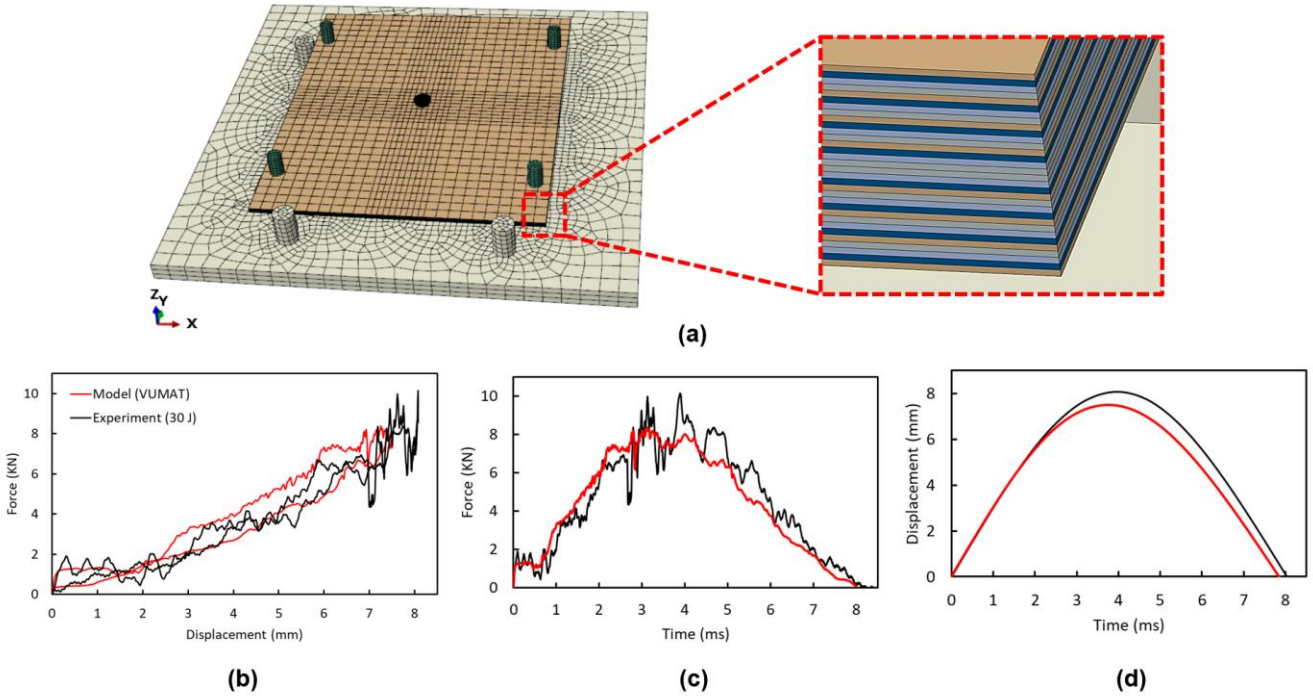

Figure 2. (a) Simplified impact model without cohesive zone elements; (b) Force-displacement curves, (c) Force-time curves, (d) Displacement-time curves of the simplified model with VUMAT subroutine of 3-D Hashin's failure criteria.

2.3 Damage Modeling Jointly Using CZM and CDM

To take advantage of both the CZM modeling technique and the CDM method to accurately capture different damage modes during the impact event, the two approaches were jointly employed to develop a high-fidelity FE model. Cohesive elements were utilized to capture delamination and intralaminar matrix cracking. Meanwhile, the

3-D Hashin's failure criteria were implemented in the solution process with a VUMAT user subroutine to capture other damage modes. In addition, an extensive parametric study was conducted to achieve a reliable and sufficiently accurate impact damage model. Some of the results will be presented in the next section.

3 RESULTS AND DISCUSSION

3.1 Comparison with Experimental Results

The FE results from the three different modeling approaches (CZM only, VUMAT only, and the combination of VUMAT and CZM) are presented in Figure 3. In the model that the damage was captured only by CZM, the maximum force was predicted correctly. However, the duration of the impact load was about one millisecond less than in the experiment. The model that only used VUMAT obtained slightly different predictions. The impact duration was estimated with satisfactory accuracy, but the maximum force was approximately 20% lower than the experimental results. The combination of these two approaches led to the results that were in between, while all the FE models exhibited underestimated maximum displacement compared with the experiment.

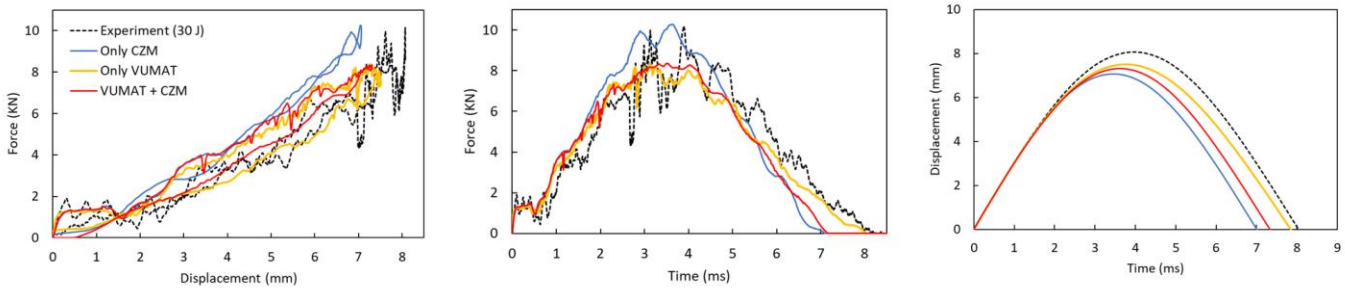

Figure 3. Impact response curves obtained from the models using three different modeling approaches.

3.2 Damaged Areas

The damaged regions at each layer are presented in Figure 4, showing fiber breakage, matrix cracking, and delamination damage modes. The images in Figure 5 represent a 40 by 40 mm region near the impactor's tip. A small area of damage (< 10 mm diameter) was captured for fiber breakage under tension, while fiber breakage under compression was limited to a few number of elements near the front surface due to the low impact energy. Regarding the matrix cracking, the damaged area enlarged from the impact front surface to the back surface of the laminate due to the higher tensile stress, which was in good agreement with the test observations. The diameter of the damaged area of matrix cracking in the last ply (ply-32) was about 35 mm. The stiffness reduction in the cohesive layers is shown in the "Delamination" section of Figure 4. With the change of the colors from blue to red, the stiffness decreased until lost completely. Thus, the delaminated regions are those regions that are indicate with the red color. Figure 5 shows the matrix cracks caught by the intralaminar cohesive elements, and the red regions indicate that matrix cracking has occurred.

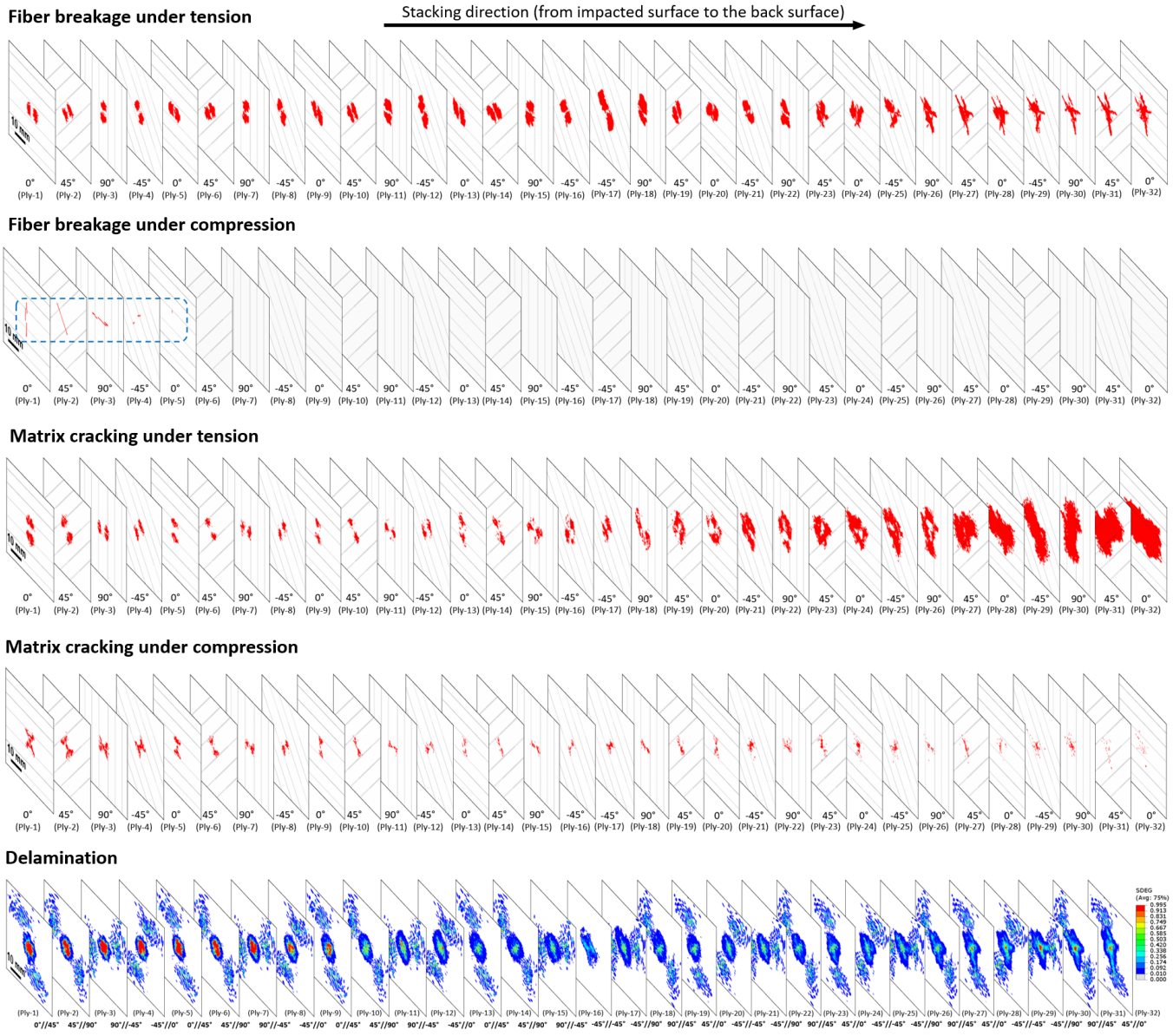

Figure 4. Damaged regions captured by VUMAT subroutine and CZM.

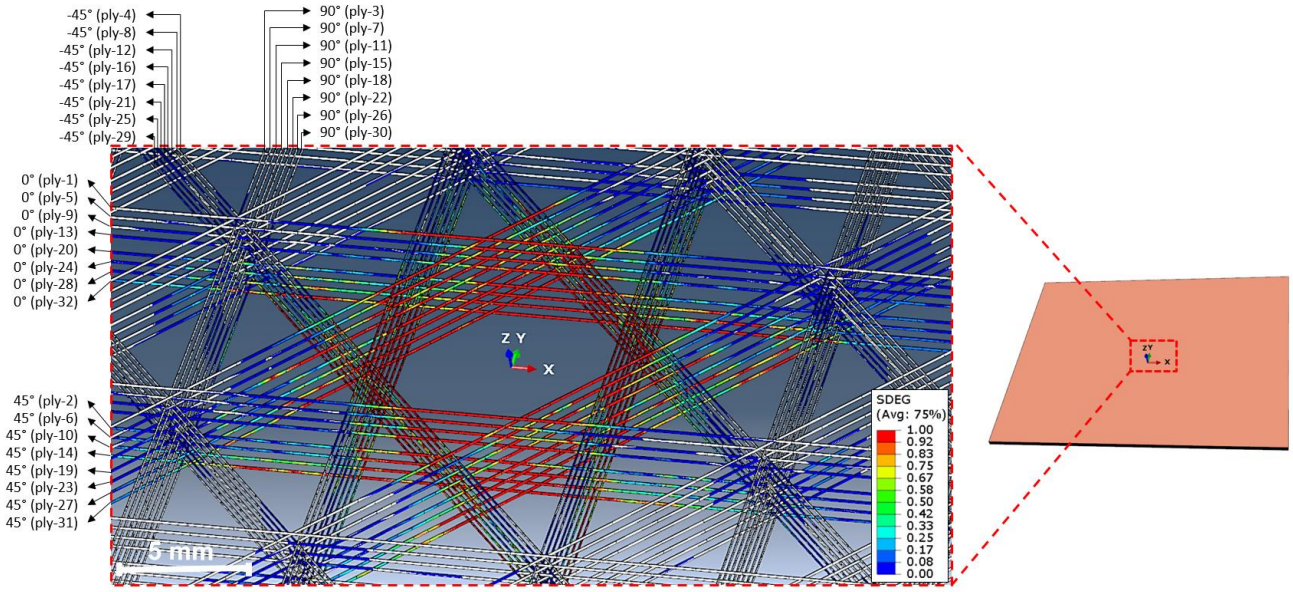

Figure 5. Matrix cracking captured by cohesive elements embedded inside each of the composite layers of the laminate.

3.3 Energy Dissipation Due To Damage

In the design stage of composite structures, knowing when and where damage may initiate and how the damage may evolve after an LVI event can be very helpful to choose a proper stacking sequence and laminate thickness. One way to monitor the evolution of different damage modes is to find the history of the dissipated energy due to damage at different regions of the laminate. For the delamination and intralaminar matrix cracking that are captured by cohesive elements, it is possible to request damage energy output variable (ALLDMD) from Abaqus. However, for the other damage modes that are caught by the VUMAT user subroutine, the corresponding dissipated damage energy cannot be directly obtained from Abaqus. Therefore, the VUMAT user subroutine was further developed to calculate the energy dissipated by each different damage mode occurred in each element. To calculate the energy dissipation in an element, three scenarios should be considered, as shown in Figure 6. The first scenario is the occurrence of matrix cracking failure in an element. After the matrix cracking, the dissipated energy would be calculated and we would observe a decrease in the stress in the fiber direction (σ_1) and a full drop in the stress in the matrix direction (σ_2). However, the element is still capable of bearing load in the fiber direction until the end of the simulation. The second scenario is the occurrence of failure only in the fiber direction (i.e. fiber breakage). In this scenario, all components of the stiffness matrix of the failed element would reduce to zero. Consequently, the stress in both fiber and matrix directions would drop to zero, and it is not possible to have matrix failure after fiber breakage. There is also another scenario in which transverse matrix cracking occurs first. At this point, the stress in the matrix direction (perpendicular to the fiber direction) would drop to zero. The stress in the fiber direction also decreases. As the strain increases, the stress in the fiber direction (σ_1) would increase until reaching the material strength in the fiber direction. Therefore, it is possible to see fiber failure in an element even after matrix cracking failure.

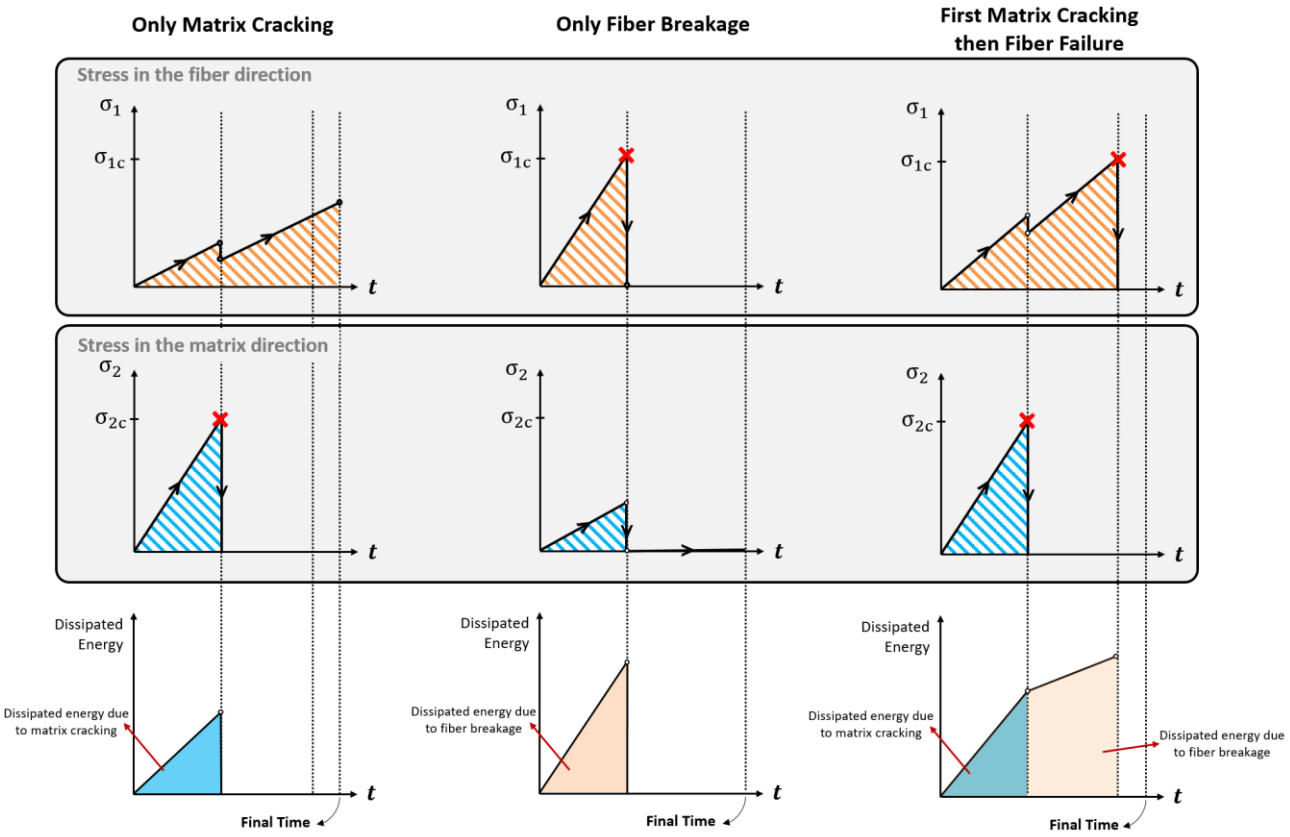

Figure 6. Damage occurrence sequences and the corresponding dissipated energies for each element.

By creating "sets" in Abaqus and monitoring the history of the dissipated damage energies, it was possible to locate the region from which the damage energy has been dissipated throughout the LVI. The results of the energy dissipation analysis are presented in Figure 7. In this figure, the major load drops in the load-time diagram are correlated to the corresponding damage mode using the dissipated energies. The first load drop was due to delamination between the plies 31 and 32. The start of intralaminar matrix cracking at plies 16, 17, 28 and 32 was also happened before the first load drop. The second drop resulted from the matrix cracking in the first two plies (near the impactor tip) and in the last four plies. The initiation of delamination between other plies of the laminate was also captured at this point. The third load drop took place mostly because of fiber breakage and matrix cracking in the layers below the neutral axis. At this point, fiber breakage and matrix cracking were also detected in the first four layers due to compressive stresses. After the fourth load drop, all damage modes contributed to enlarging the damaged areas.

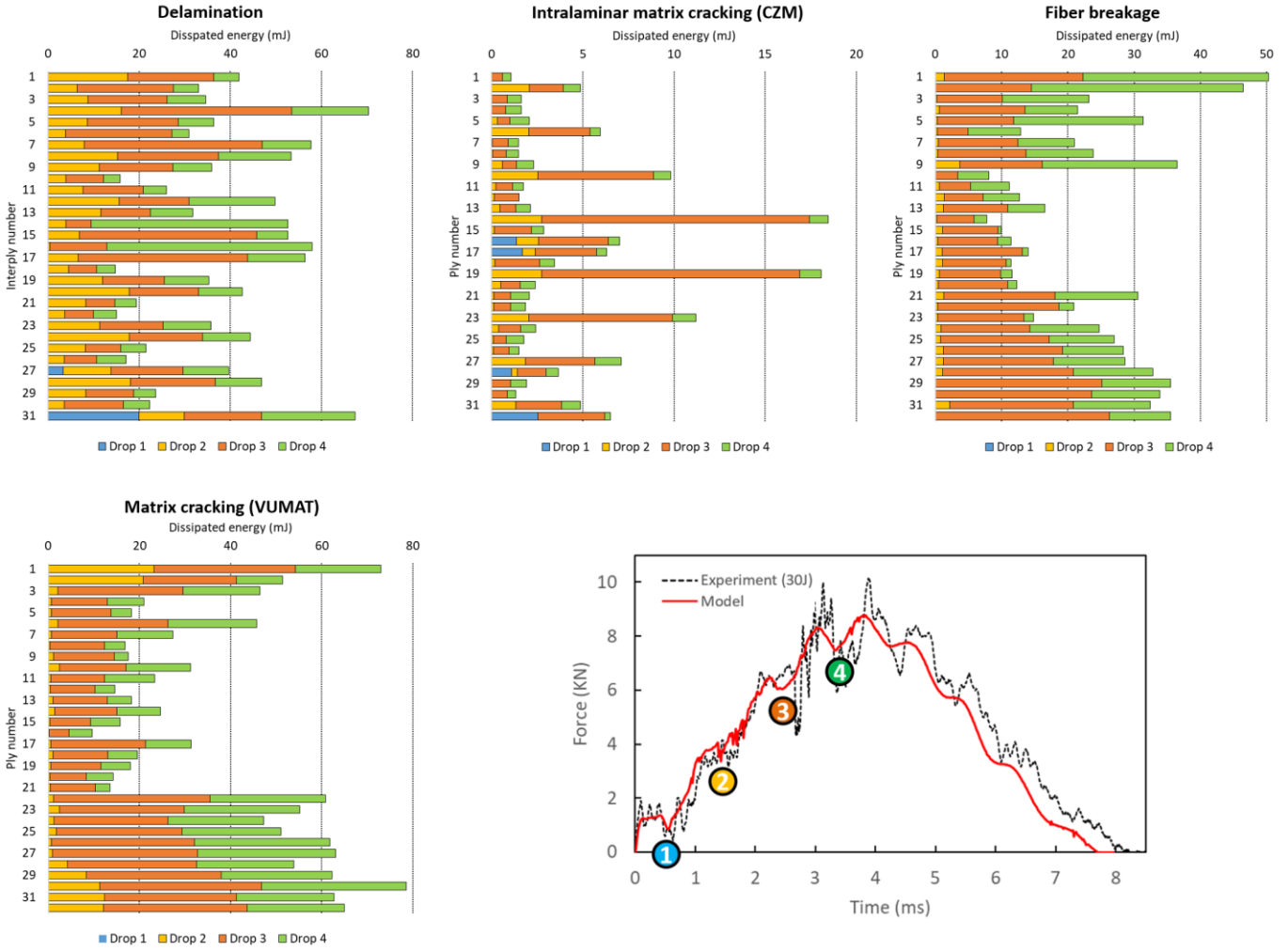

Figure 7. Force-time response of the laminate subjected to impact with 30 J energy, and dissipated energies corresponding to the indicated drops due to fiber breakage, delamination and matrix cracking. Ply 1 is on the front surface of the laminate and ply 32 is on the back.

4 CONCLUSION

Finite element modeling and simulation for a carbon fiber-reinforced composite laminate under a low-velocity impact (LVI) was conducted. Compared with the experimental results, the approach that combined the cohesive zone method (CZM) and continuum damage mechanics (CDM) was proven an effective methodology to predict the complex damage behavior of the structure and monitor the damage evolution inside the laminate. In this study, cohesive elements were used to model delamination and intralaminar matrix cracking, while fiber breakage and transverse matrix cracking were captured by a VUMAT user subroutine written based on the 3-D Hashin's composite failure criteria. By calculating the dissipated energies due to different damage modes, the damage sequence throughout the LVI event was predicted. Although in this study the method of calculating dissipated energy was used only for tracing damage occurred during the LVI, the same approach can be used in the design stage of a composite structure to find the locations and modes of premature damage, and to improve the design (stacking sequence or geometry) in such a way to postpone the damage initiation.

5 REFERENCES

[1] A. Trellu, C. Bouvet, S. Rivallant, and L. Ratsifandrihana, "A new interface element connecting 3D finite elements with non-coincident nodes to simulate delamination in composite laminates." *Composite Structures*, vol. 252, p. 112694, 2020.

[2] H. Tuo, Z. Lu, X. Ma, C. Zhang, and S. Chen, "An experimental and numerical investigation on low-velocity impact damage and compression-after-impact behavior of composite laminates," *Composites Part B: Engineering*, vol. 167, pp. 329–341, 2019.

[3] W. Tan, B. G. Falzon, L. N. S. Chiu, and M. Price, "Predicting low velocity impact damage and Compression-After-Impact (CAI) behaviour of composite laminates," *Composites Part A: Applied Science and Manufacturing*, vol. 71, pp. 212–226, 2015.

[4] E. V González, P. Maimí, P. P. Camanho, A. Turon, and J. A. Mayugo, "Simulation of drop-weight impact and compression after impact tests on composite laminates," *Composite Structures*, vol. 94, no. 11, pp. 3364–3378, 2012.

[5] H. Liu, B. G. Falzon, and W. Tan, "Experimental and numerical studies on the impact response of damage-tolerant hybrid unidirectional/woven carbon-fibre reinforced composite laminates," *Composites Part B: Engineering*, vol. 136, pp. 101–118, 2018.

[6] A. Soto, E. V González, P. Maimí, F. M. De La Escalera, J. R. S. De Aja, and E. Alvarez, "Low velocity impact and compression after impact simulation of thin ply laminates," *Composites Part A: Applied Science and Manufacturing*, vol. 109, pp. 413–427, 2018.

[7] D. C. Pham, J. Lua, H. Sun, and D. Zhang, "A three-dimensional progressive damage model for drop-weight impact and compression after impact," *Journal of Composite Materials*, vol. 54, no. 4, pp. 449–462, 2020.

[8] J. Reiner and R. Vaziri, "Local and nonlocal continuum damage simulation of impact and compression after impact tests on CFRP laminates," The 22th International Conference on Cmposite Materials (ICCM22), Melbourne, Australia, 2019.

[9] R. Borrelli, S. Franchitti, F. Di Caprio, F. Romano, and U. Mercurio, "A numerical procedure for the virtual compression after impact analysis," *Advanced Composites Letters*, vol. 24, no. 4, p. 096369351502400401, 2015.

[10] S. Rivallant, C. Bouvet, and N. Hongkarnjanakul, "Failure analysis of CFRP laminates subjected to compression after impact: FE simulation using discrete interface elements," *Composites Part A: Applied Science and Manufacturing*, vol. 55, pp. 83–93, 2013.

[11] M. R. Abir, T. E. Tay, M. Ridha, and H. P. Lee, "On the relationship between failure mechanism and compression after impact (CAI) strength in composites," *Composite Structures*, vol. 182, no. September, pp. 242–250, 2017.

[12] H. Abdulhamid, C. Bouvet, L. Michel, J. Aboissiere, and C. Minot, "Numerical simulation of impact and compression after impact of asymmetrically tapered laminated CFRP," *International Journal of Impact Engineering*, vol. 95, pp. 154–164, 2016.

[13] T. D. Dang, S. R. Hallet, B. C. Kim, Y. Le Cahain, R. Butler, and W. Liu, "Modelling of as manufactured geometry for prediction of impact and compression after impact behaviour of variable angle tow laminates," *Journal of Composite Materials*, vol. 49, no. 12, pp. 1423–1438, 2015.

[14] H. Tuo, Z. Lu, X. Ma, J. Xing, and C. Zhang, "Damage and failure mechanism of thin composite laminates under low-velocity impact and compression-after-impact loading conditions," *Composites Part B: Engineering*, vol. 163, pp. 642–654, 2019.

[15] X. C. Sun and S. R. Hallett, "Failure mechanisms and damage evolution of laminated composites under compression after impact (CAI): Experimental and numerical study," *Composites Part A: Applied Science and Manufacturing*, vol. 104, pp. 41–59, 2018.

[16] N. Dubary, C. Bouvet, S. Rivallant, and L. Ratsifandrihana, "Damage tolerance of an impacted composite laminate," *Composite Structures*, vol. 206, pp. 261–271, 2018.

[17] Z. Hashin, "Failure criteria for unidirectional fiber composites," *Journal of Applied Mechanics*, vol. 47, pp. 329–334, 1980.